

## Original Research Article

# Structure delineation in the presence of metal – A comparative phantom study using single and dual-energy computed tomography with and without metal artefact reduction



Erik Pettersson<sup>a,b,c,\*</sup>, Anna Bäck<sup>b,c</sup>, Thomas Björk-Eriksson<sup>d,e</sup>, Ulrika Lindencrona<sup>b,c</sup>, Karin Petruson<sup>f</sup>, Anne Thilander-Klang<sup>a,c</sup>

<sup>a</sup> Department of Diagnostic Radiation Physics, Medical Physics and Biomedical Engineering, Sahlgrenska University Hospital, SE-41345 Gothenburg, Sweden

<sup>b</sup> Department of Therapeutic Radiation Physics, Medical Physics and Biomedical Engineering, Sahlgrenska University Hospital, SE-41345 Gothenburg, Sweden

<sup>c</sup> Department of Radiation Physics, Institute of Clinical Sciences, Sahlgrenska Academy, University of Gothenburg, SE-41345 Gothenburg, Sweden

<sup>d</sup> Department of Oncology, Institute of Clinical Sciences, Sahlgrenska Academy, University of Gothenburg, SE-41345 Gothenburg, Sweden

<sup>e</sup> Regional Cancer Center West, Sahlgrenska University Hospital, SE-41345 Gothenburg, Sweden

<sup>f</sup> Department of Oncology, Sahlgrenska University Hospital, SE-41345 Gothenburg, Sweden

## ARTICLE INFO

## Keywords:

Radiotherapy  
Treatment planning  
Computed tomography  
Delineation uncertainty  
Dual-energy computed tomography  
Metal artefact reduction

## ABSTRACT

**Background and purpose:** Metal artefacts in computed tomography (CT) images impairs structure delineation. These artefacts can potentially be reduced with dual-energy CT (DECT) with or without using metal artefact reduction (MAR). The purpose was to investigate how structure delineation in DECT with or without MAR and single-energy CT (SECT) images were affected by metals.

**Materials and methods:** A phantom with known irregular structures was developed. Reference structures were determined from a low-noise scan without metal. Bilateral hip prostheses were simulated with steel or titanium inserts. The phantom was scanned with SECT and fast-kV switching DECT with optional MAR. Four radiation oncologists delineated the structures in two phantom set-ups. Delineated structures were evaluated with Dice similarity coefficient (DSC) and Hausdorff distance relative to the reference structures.

**Results:** With titanium inserts, more structures were detected for non-MAR DECT compared to SECT while the same or less were detected with steel inserts. MAR improved delineation in DECT images. For steel inserts, three structures in the region of artefacts, were delineated by at least two oncologists with MAR-DECT compared to none with non-MAR DECT or SECT. The highest values of DSC for MAR-DECT were 0.69, 0.81 and 0.77 for those structures.

**Conclusions:** Delineation was improved with non-MAR DECT compared to SECT, especially for titanium inserts. A larger improvement was seen with the use of MAR for both steel and titanium inserts. The improvement was dependent on the location of the structure relative to the inserts, and the structure contrast relative to the background.

## 1. Introduction

In radiotherapy planning, the target volumes and the organ at risk (OARs) volumes are delineated using computed tomography (CT) images or magnetic resonance imaging (MRI). Based on these delineations, treatment is optimised to ensure the prescribed absorbed dose to the target volumes, while minimizing the delivered dose to the OARs.

Metal implants, e.g. hip prostheses or dental amalgam fillings, will

lead to artefacts in CT images caused by beam hardening and photon starvation [1]. Such artefacts can reduce the visibility of organs/structures, thus affecting the ability to delineate the structures close to the implants. Today, the delineation of target structures and OARs is often performed using MRI rather than CT due to the superior soft-tissue contrast of MRI [2]. MRI is also affected by metal implants. Furthermore, MRI is impracticable for some patients with certain types of ferromagnetic metal implants and can be unworkable for patients

\* Corresponding author at: Department of Therapeutic Radiation Physics, Medical Physics and Biomedical Engineering, Sahlgrenska University Hospital, SE-41345 Gothenburg, Sweden.

E-mail addresses: [erik.a.pettersson@vgregion.se](mailto:erik.a.pettersson@vgregion.se) (E. Pettersson), [anna.back@vgregion.se](mailto:anna.back@vgregion.se) (A. Bäck), [thomas.bjork-eriksson@rccvast.se](mailto:thomas.bjork-eriksson@rccvast.se) (T. Björk-Eriksson), [ulrika.lindencrona@vgregion.se](mailto:ulrika.lindencrona@vgregion.se) (U. Lindencrona), [karin.petruson@vgregion.se](mailto:karin.petruson@vgregion.se) (K. Petruson), [anne.thilander-klang@vgregion.se](mailto:anne.thilander-klang@vgregion.se) (A. Thilander-Klang).

<https://doi.org/10.1016/j.phro.2019.01.001>

Received 26 June 2018; Received in revised form 4 December 2018; Accepted 10 January 2019

2405-6316/© 2019 The Authors. Published by Elsevier B.V. on behalf of European Society of Radiotherapy & Oncology. This is an open access article under the CC BY-NC-ND license (<http://creativecommons.org/licenses/by-nc-nd/4.0/>).

with a pacemaker or patients suffering from claustrophobia. Therefore, CT is still needed for radiotherapy target delineation, and metal artefacts in CT images still pose a problem for delineation. Furthermore, when dose calculations are based on CT images, artefacts from metal implants cause uncertainties [3,4].

Most CT scanner manufacturers provide a metal artefact reduction (MAR) algorithm, which to different degree reduce the metal artefacts in CT images. In general, MAR methods replace the projections passing through metal with interpolated data from neighbouring projections [5]. Metal artefacts can also be reduced using dual-energy CT (DECT) [3,6,7,8,9], which exploit the energy dependence of the attenuation coefficients to quantify the material with higher accuracy compared to single-energy CT (SECT), e.g. by scanning at two tube voltages, or by using energy-discriminating detectors. It is important to optimize the CT technique used for structure delineation and radiotherapy treatment planning for patients with metal implants.

Few comparative studies have been carried out on structure delineation in the presence of metal artefacts in images based on the fast kV-switching (FKS) DECT technique. This projection based DECT technique is in theory free from beam hardening effects [10,11] and less sensitive to patient motion compared to the DECT with sequential scans. FKS-DECT in combination with MAR have been reported to improve image quality and delineation in patients [12] and tissue quantification in phantoms [13] by reducing artefacts from dental metal implants. However, additional artefacts can be introduced by the MAR algorithm itself [7,12,13]. A recent study by Kovacs et al. [14] reported that DECT with sequential scans and MAR improved the delineations accuracy in both phantoms and patients, compared to SECT.

The present study investigated how artefacts from different metals, simulating bilateral hip prostheses, affect the delineation of irregular known structures of different CT numbers using FKS-DECT with and without MAR and also compared to SECT.

## 2. Materials and methods

### 2.1. The phantom

An electron density phantom (062M, CIRS Inc., Norfolk, USA) made of Plastic Water™, measuring 33 cm × 27 cm × 5 cm, was used. Cylindrical tissue surrogate inserts, 3 cm in diameter and 5 cm long, covering a range of electron densities normally found in the human body, can be used with this phantom (see Fig. 1, left). To study the effects of metal implants, in-house manufactured inserts of steel and titanium were inserted in the most lateral positions of the phantom to simulate bilateral hip prostheses [8]. Polymethylmethacrylate (PMMA) inserts were used in the non-metal phantom configurations. Tissue surrogate inserts with different densities were inserted in the other outer six positions of the phantom (Fig. 1). To achieve patient-like scattering conditions in the CT scanners, 10 cm Plastic Water™ slabs

were placed cranially and caudally of the 5 cm thick phantom section.

The central cylindrical insert (diameter 18 cm) of the phantom was replaced with a polyethylene cylinder containing irregularly shaped structures with different contrast to the surrounding homogeneous gelatine (Fig. 1). The CT number differences of the structures compared to the surrounding gelatine were generated to, as good as possible, approximately mirror those of tissues found in the pelvic region. The production of the structures is described in Appendix A. Structure 1, 2, 3 and 5 were 1.5 cm thick in the cranio-caudal direction and structure 4 were shaped as a 2 cm diameter sphere. The most cranial part of the structures were placed in the same transversal plane of the phantom.

Our version of the 062M phantom allows for the central insert to be rotated, allowing the position of the structures in the cylinder to be changed in relation to the metal inserts. All CT scans were repeated with two set-ups of the phantom (A and B) where the cylinder was rotated approximately 90 degrees.

### 2.2. CT scanning

Two CT scanners were used, a SECT scanner normally used for radiotherapy treatment planning (Aquilion Large Bore, Toshiba Medical Systems, Tokyo, Japan), and a diagnostic DECT scanner (Discovery CT750 HD, GE Healthcare, Waukesha, USA) capable of both SECT and FKS-DECT scanning (Gemstone Spectral Imaging™, GE Healthcare, Waukesha, USA). The phantom was scanned at set-up A and B consecutively on each CT scanner, and scans were performed on two consecutive days, one for each scanner. For each scanner and phantom set-up, three scans were performed with either steel, titanium or PMMA inserts. Image series were produced with the SECT scanner using a tube voltage of 120 kV. With the DECT scan mode on the DECT scanner, virtually monoenergetic image series were reconstructed at photon energies of 70 keV and 110 keV. The DECT image series were reconstructed with and without the optional MAR software (MARs™, GE Healthcare, Waukesha, USA). The 70 keV non-MAR image series with the titanium inserts were, based on an earlier study [8] deemed similar to those with steel inserts and were therefore excluded from the study to limit the total number of image series.

Two additional SECT scans with the PMMA inserts, one for each phantom set-up, were performed with the DECT scanner to create reference image series. These scans were not clinically relevant but were produced to give the best possible image quality for the determination of the reference structures. The oncologists were also asked to also perform delineations in these image series which were evaluated together with the other image series. These reference image series were taken at 120 kV and reconstructed with a noise-reducing model-based iterative reconstruction algorithm (Veo™, GE Healthcare, Waukesha, USA) [15]. A reduced display-field-of-view were used to increase the accuracy of delineation.

In total, 26 image series were reconstructed from 14 scans. The

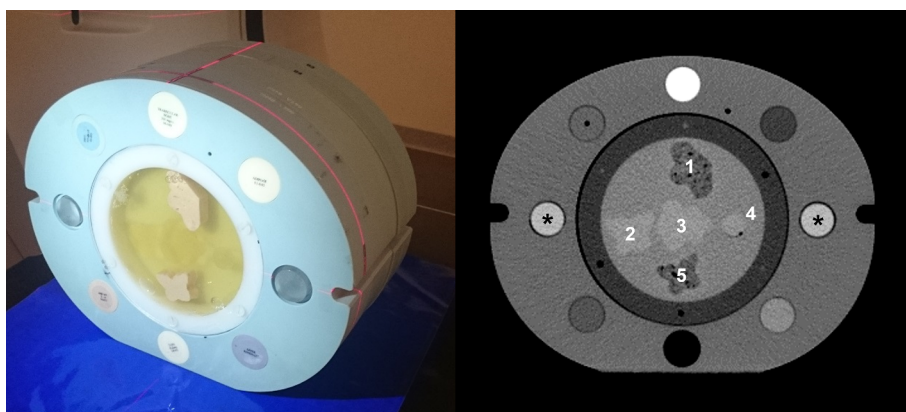


Fig. 1. Left: A photograph of the phantom with the central cylinder containing five structures denoted 1 to 5 in homogeneous gelatine. Tissue surrogate inserts with six different mass densities, lung exhale (0.50 g/cm<sup>3</sup>), adipose (0.96 g/cm<sup>3</sup>), breast (0.99 g/cm<sup>3</sup>), plastic water (1.03 g/cm<sup>3</sup>), liver (1.07 g/cm<sup>3</sup>) and trabecular bone (1.16 g/cm<sup>3</sup>) were inserted in the six frontal and dorsal positions of the phantom. Ten cm of plastic water slabs were placed in both the cranial and caudal direction of the central electron density phantom during the CT scans. The caudal slabs are not present in the photograph. Right: A SECT image of the phantom acquired with PMMA inserts in the lateral positions (A10) with display window level and width set to 40 HU and 400 HU, respectively. The two PMMA cylinders are marked with asterisks (\*).

**Table 1**  
The scanning and reconstruction parameters used for the SECT and DECT scanners.

Scanner	Tube voltage (kV)	Scan mode (Bow-tie filter)	Helical pitch	Tube current [mA]	Rotation time [s]	SFOV [cm]	DFOV [cm]	Beam collimation [mm]	Slice thickness [mm]	Convolution kernel	CTDI <sub>vol,32cm</sub> [mGy]
SECT	120	LL	0.938	125	0.5	55	55	32	3.0	FC17	14.5
DECT	80/140	Body	0.969	225	0.6	50	50	40	2.5	Standard	13.84
Ref.*	120	Body	0.969	525	1	50	25	40	2.5	Standard	47

SFOV = scan field of view, DFOV = display field of view, CTDI<sub>vol,32cm</sub> = volumetric CT dose index in the 32 cm phantom.

\* The high-dose SECT scan acquired with the DECT scanner used to reconstruct the low-noise reference images.

regular clinical scanning protocol was used for the SECT scanner. The DECT scans were forced to be used with a pre-set GSI scan protocol that defined the scan parameters. The GSI scan protocol used in this study, i.e. GSI-33, was chosen due to the resemblance with the SECT protocol. All scan and reconstruction parameters are given in Table 1. The slices in each image series used for delineation were limited to those in the cranial-caudal direction containing the structures plus two additional slices in each of the cranial and caudal direction. The image series from the DECT and SECT comprised twelve and eleven slices, respectively, due to differences in image slice thickness (Table 1).

### 2.3. Delineation

Delineation was performed independently by four radiation oncologists with; 25, 7, 1 and 1 years of experience in clinical target delineation. They were informed that they were to review a sequence of 13 series of images for each phantom set-up, each containing an unknown number of structures. The oncologists were instructed to delineate the structures that they could identify in each image, as thoroughly as reasonably possible, using the delineation technique they were accustomed to in the clinical treatment planning system (TPS) (Eclipse™ 11.0, Varian Medical Systems, Palo Alto, USA). Changing window level and window width was allowed. As the oncologists were to delineate the same structures in different images series, the 13 image series for each phantom set-up were presented according to the severity of beam-hardening artefacts and correlated noise in the images, starting with the most severe artefacts and progressing to low noise images (Table 2 and Fig. 2). This sequence was chosen to minimise information from previous images from influencing the delineation in subsequent images. Identical sequences were used for set-up A and B. The oncologists were instructed not to return to already delineated image series. All image series from set-up A were delineated first and image series from set-up B were delineated approximately one week after. Hereafter, the notation A1-A13 and B1-B13 for the different image series is used according to Table 2.

Two reference structure sets were created in the TPS using CT number thresholding in the reference image series A13 and B13. Thresholding was performed inside a user-defined cuboid region completely covering one structure at a time. Any jagged edges, internal cavities or outlying pixels located far away from the main structure caused by thresholding were removed. Any air pockets on the surface of

**Table 2**

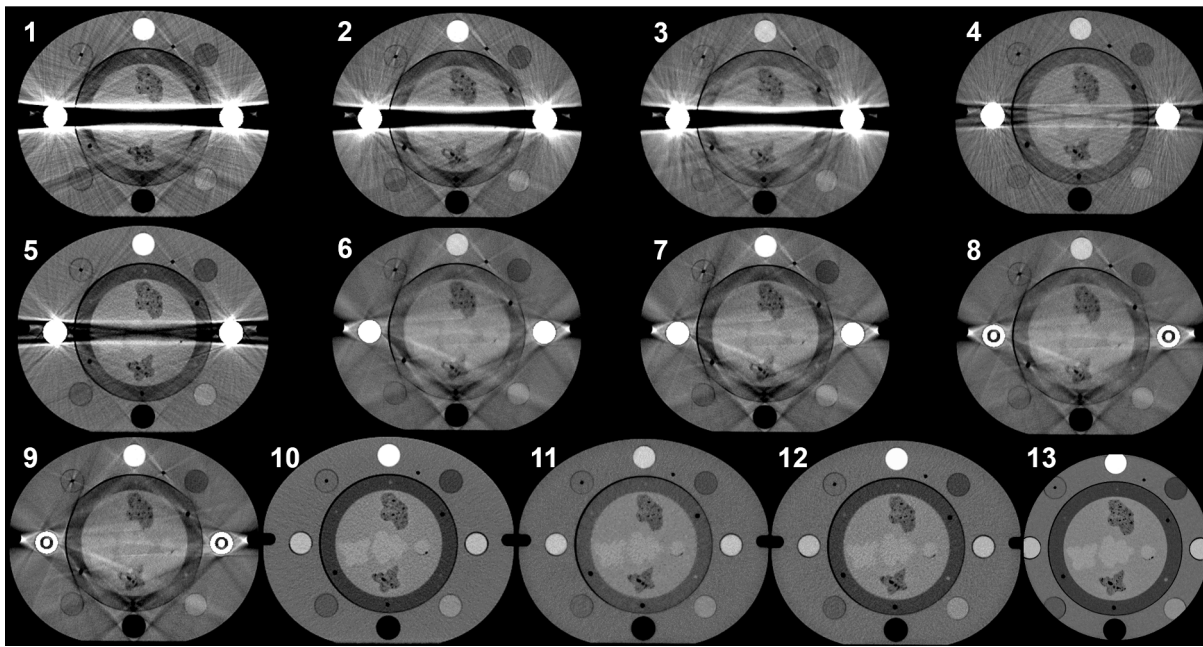
The sequence of image series in which the four radiation oncologists delineated the structures in the phantom. The image series were presented in descending degree of metal artefacts. This sequence were used for both phantom set-up A and B.

Image series	Scanner	Properties*	Metal artefact reduction	Lateral insert material
1	SECT	120 kV	–	Steel
2	DECT	70 keV	No	Steel
3	DECT	110 keV	No	Steel
4	DECT	110 keV	No	Titanium
5	SECT	120 kV	–	Titanium
6	DECT	110 keV	Yes	Steel
7	DECT	70 keV	Yes	Steel
8	DECT	110 keV	Yes	Titanium
9	DECT	70 keV	Yes	Titanium
10	SECT	120 kV	–	PMMA
11	DECT	110 keV	No	PMMA
12	DECT	70 keV	No	PMMA
13	Ref.	120 kV, MBIR	–	PMMA

\* kV indicates polychromatic X-ray spectra, while keV indicates virtually monoenergetic energy resulting from dual-energy CT scanning.

The Ref. image series was a high dose SECT scan acquired with the DECT scanner.

MBIR = model-based iterative reconstruction.



**Fig. 2.** The central slice in each of the image series of phantom set-up A (A1–A13). The image series were ordered in a sequence of decreasing severity of metal artefacts. Image series number 13 does not depict the whole phantom as it was reconstructed with a reduced display field of view of 25 cm. The same sequence was used for both phantom set-ups.

the structures were included in the structures, as they deviated from the otherwise homogeneous gelatine background. The threshold levels were determined after measurement of the mean CT numbers in structure 1, 3, and in the gelatine background. These measurements were performed in a 20 mm diameter circular ROIs using ImageJ software (ImageJ, National Institutes of Health, Bethesda, USA) in the central slice of the reference image series A13.

#### 2.4. Evaluation

Each image series was geometrically matched to the corresponding reference image series (A13 and B13) using rigid registrations in the software Velocity AI™ 3.2 (Varian Medical Systems, Palo Alto, USA). When a delineation coincided with a reference structure, it was tallied as a delineated structure, and was compared to that reference structure using the Dice similarity coefficient (DSC) [16] and the Hausdorff distance (HD) [17]. The DSC is a measure of the geometric overlap of two volumes  $X$  and  $Y$ , and is equal to their intersection ( $|X \cap Y|$ ) divided by their mean volume. The HD is the largest deviation in distance between the contours of a delineated volume and the nearest point on the contour at its reference volume. The DSCs and HDs were calculated using the TPS and Velocity AI software, respectively.

### 3. Results

The mean CT numbers in structure 1, 3, and the gelatine background measured in image series A13 were  $-19$ ,  $70$  and  $39$  Hounsfield Units (HU), respectively. The reference structures were thresholded using CT numbers above  $57$  HU for structures 2, 3 and 4, and below  $20$  HU for structures 1 and 5. These are presented together with the oncologists' delineations for phantom set-up A in Fig. 3 and for B in Appendix B.

The oncologists' delineation in the reference scans (A13, B13), resulted in values of  $DSC \geq 0.83$ , see Fig. 4 where the number of delineations per structure, minimum and maximum values of both DSC and HD for the five delineated structures by the four radiation oncologists are presented.

In general, structures with a higher contrast to the background were

more often correctly detected than structures with lower contrast. For example, structure 1 and 5 were delineated by all four oncologists in all image series, except in those with steel inserts in set-up B when not using MAR. Structure 2, 3 and 4 were detected by all oncologists only in the image series with PMMA inserts. Between steel inserts for set-up A, structure 2, 3 and 4 were only delineated in the image series using MAR but not by all oncologists. For set-up B, at least two oncologists delineated structure 1 and 5 between steel inserts also in image series without MAR, while structure 3 was undetected in those images.

The differences between the SECT and DECT techniques were not pronounced with steel inserts. With titanium inserts, structure 3 was delineated by three oncologists for non-MAR DECT (A4 and B4), compared to one for SECT (A5 and B5). The values of DSC and HD were in those cases always worse for SECT except for the DSC value for phantom set-up A, but then still in the lower range of DSC values for the non-MAR DECT.

MAR improved structure delineation between the metal inserts in images from the DECT scanner. For example, structure 2, 3 and 4, situated between steel inserts (phantom set-up A) were delineated by at least two oncologists with  $70$  keV MAR-DECT (A7), compared to none for non-MAR DECT (A2–A3). The highest value of DSC for MAR-DECT were in those cases  $0.69$ ,  $0.81$  and  $0.77$  for the structure 2, 3 and 4 respectively. The effect of MAR was smaller for titanium compared to steel inserts where for example structure 5 was delineated by all oncologists for titanium inserts already without using MAR.

In some cases MAR aggravated structure delineation. Structure 4 in set-up B, placed dorsally of the metal inserts, was delineated by all oncologists in both SECT and non-MAR DECT images (B1–B5), compared to by only three with DECT-MAR (B6–B9).

In two cases with steel inserts, for non-MAR DECT  $110$  keV (A3) and DECT-MAR  $70$  keV (A7), a HD above  $30$  mm was found for structure 5 although the DSC ranged from  $0.62$  to  $0.85$  and  $0.77$ – $0.85$  for those cases.

### 4. Discussion

In this study we have evaluated how metal artefacts in CT images affect the delineation of structures in images from a SECT scanner used

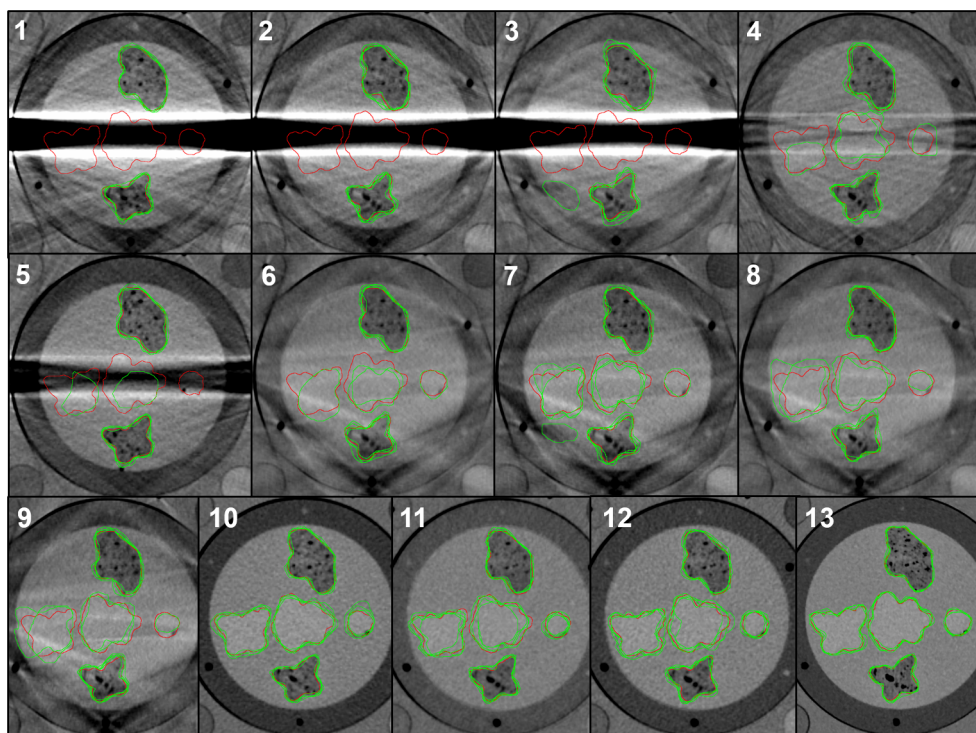


**Fig. 3.** The contours delineated by the four radiation oncologists (green) and the reference contours (red) in the central image slice of each of the 13 image series in phantom set-up A. For each phantom set-up, image series 13 was also used to create the red reference contours. Only the central part of the phantom is displayed in the figure, but the oncologists were shown the whole images. For the corresponding figure with set-up B, see [Fig. B.1 in the supplementary material](#). (For interpretation of the references to colour in this figure legend, the reader is referred to the web version of this article.)

for radiotherapy treatment planning compared to a diagnostic CT scanner equipped with FKS-DECT, with and without MAR. Studies on the influence of metal artefacts on structure delineation are scarce. In one recent study, Kovacs et al. [14] showed that the use of DECT with sequential SECT scans together with MAR improved the accuracy of delineations in comparison to non-MAR DECT for a phantom with artefacts resulting from a hip implant. Our study focus on a different DECT technique and in our case, the FKS scan mode was a prerequisite for the MAR algorithm, and thus not available for any SECT scan in this study. The structures in the phantom were designed to mimic the image contrast of human tissues. Structure 1 and 5 had a contrast to the background similar to that of adipose tissue to muscle. Structure 2, 3 and 4 had a contrast to the background similar to that of the peripheral to the central zones of the prostate [18]. The study was designed to be based on a quantitative analysis and the oncologists were not asked to give any information on their subjective perception on the visibility of the structures in the images.

To minimize the delineation bias from previous delineations, the image series were presented in the order from more severe artefacts to less severe artefacts, similar to the method of Kovacs [14]. Furthermore, the oncologists did not get any information about that the same phantom and structures were used throughout the series or between the two phantom set-ups. Although, there might be a delineation bias because of knowledge about the phantom and structures gained from previous images in the delineation series both within the series and between the two phantom set-ups.

In the reference image series the minimum DSC was 0.83, implying that higher values could be regarded as within the uncertainty of manual delineation of visible structures. Although the DSC of a delineated structure may be within the uncertainty for manual delineation in comparison with the reference structure, the value of HD for the same structure could be several mm. The DSC was used in combination with the HD, which is common in delineation studies [19]. For two image series a part of an artefact was included in structure 5 as a protuberance (A3) and as an additional structure (A7). The DSCs for

these cases ranged from 0.62 to 0.85 while the maximum HD were larger than 30 mm, demonstrating the value of the HD as a compliment to the DSC in delineation studies.

The results of this study showed that DECT combined with MAR improved the delineation accuracy in many cases with titanium or steel inserts compared to SECT or non-MAR DECT. The geometries of the metal inserts were identical, therefore the results in metal artefacts reflect the differences between titanium and steel. Metal hip prosthesis used in patients are larger than the metal inserts used in this study, and the effects of artefacts from metal in a clinical setting can therefore be expected to be greater than those reported in this study.

The number of delineated structures between titanium inserts were higher in non-MAR DECT images compared to SECT. Although the number of delineations were similar between with/without MAR DECT, the DSCs were higher with MAR. Apart from the higher contrast to the background for structure 1 and 5, the heterogeneities in the structures, and the fact that they had a lower CT number than the background (i.e. appeared darker than the background) might also have contributed to making them somewhat easier to identify.

Our study demonstrates the clinical potential for the FKS-DECT with MAR when delineating structures. It would therefore be valuable to include this image technique in the clinical workflow of radiation therapy. MAR-induced artefacts were observed which in some cases deteriorated the delineation of structures. Other studies have also reported MAR-induced artefacts [7,12]. For clinical implementation, caution should be taken regarding possible effects of MAR-induced artefacts.

In conclusion, non-MAR DECT was shown to improve the delineation of structures compared to SECT in the case of titanium inserts. In the case of steel inserts, there were only slight improvements with non-MAR DECT compared to SECT. DECT with MAR improved the structure delineations between both steel and titanium inserts compared to both SECT and non-MAR DECT. The improvement was dependent on the location of the structure relative to the inserts, and the structure contrast relative to the background.

(a)

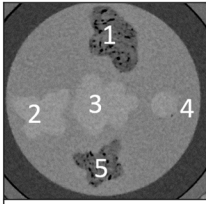


Image series, scanner, and properties.	A1, SECT, 120 kV	A2, DECT, 70 keV	A3, DECT, 110 keV	A4, DECT, 110 keV	A5, SECT, 120 kV	A6, DECT, MAR 110 keV	A7, DECT, MAR 70 keV	A8, DECT, MAR 110 keV	A9, DECT, MAR 70 keV	A10, SECT, 120 kV	A11, DECT, 110 keV	A12, DECT, 70 keV	A13, Reference, 120 kV
	Steel		Titanium		Steel		Titanium		PMMA				
Number of delineations	Structure 1	4	4	4	4	4	4	4	4	4	4	4	4
	Structure 2	0	0	0	2	1	2	3	2	2	4	4	4
	Structure 3	0	0	0	3	1	2	3	2	2	4	4	4
	Structure 4	0	0	0	1	0	1	2	1	2	4	4	4
	Structure 5	4	4	4	4	4	4	4	4	4	4	4	4
Dice similarity coefficient [max min]	Structure 1	0.90 0.84	0.88 0.83	0.88 0.84	0.89 0.87	0.85 0.83	0.90 0.87	0.91 0.87	0.88 0.86	0.89 0.85	0.88 0.84	0.89 0.87	0.94 0.87
	Structure 2				0.61 0.04	0.47 0.04	0.66 0.25	0.69 0.52	0.74 0.66	0.72 0.69	0.84 0.82	0.85 0.82	0.89 0.78
	Structure 3				0.77 0.24	0.38 0.39	0.81 0.65	0.81 0.67	0.73 0.75	0.87 0.75	0.85 0.61	0.88 0.72	0.89 0.78
	Structure 4				0.58		0.78	0.77 0.23	0.57 0.03	0.73 0.73	0.79 0.43	0.83 0.53	0.83 0.71
	Structure 5	0.80 0.75	0.86 0.76	0.85 0.62	0.87 0.80	0.77 0.76	0.85 0.59	0.85 0.77	0.87 0.81	0.87 0.80	0.80 0.76	0.88 0.85	0.87 0.84
Hausdorff distance [mm] [max min]	Structure 1	8.6 3.8	8.3 5.6	6.3 4.9	8.1 5.1	8.1 5.2	4.9 3.9	5.4 4.3	5.8 4.3	7.8 3.4	5.5 5.0	6.1 3.9	5.5 4.3
	Structure 2				26.5 15.6	20.8	24.5 14.4	13.8 10.8	11.1 9.0	10.7 10.5	6.4 4.5	7.3 5.0	7.0 4.8
	Structure 3				14.3 8.3	18.4	13.5 10.3	8.3 6.3	7.7 7.3	7.8 5.4	7.2 4.5	7.8 5.9	6.1 4.6
	Structure 4				12.8		6.2	10.5 5.0	5.0	18.6 5.0	8.5 3.5	10.0 3.1	5.2 2.9
	Structure 5	8.4 5.0	19.1 4.8	39.7 8.3	7.3 2.9	7.3 5.0	14.0 5.9	32.2 6.6	10.3 5.8	8.8 5.0	6.0 5.0	5.4 3.9	6.0 3.4

Fig. 4. Delineation of all structures (1–5) by all four radiation oncologists, for the 13 image series with the set-up A (a) and B (b). The numbering of the structures is given in the image in the top left corners. The colours in the cells indicate how many of the four radiation oncologists that delineated each structure in each image series (white = 0, red = 1, orange = 2, yellow = 3, green = 4). The minimum and maximum values of the corresponding Dice similarity coefficients and Hausdorff distances for each structure and image series, are given with the colour scheme described above for each phantom set-up. Reference denotes the SECT scans performed with the DECT scanner, these image series (A13 and B13) were used to create a reference structure sets. (For interpretation of the references to colour in this figure legend, the reader is referred to the web version of this article.)

(b)

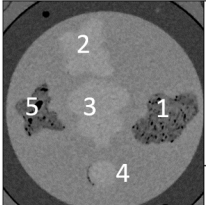


Image series, scanner, and properties.	B1, SECT, 120 kV	B2, DECT, 70 keV	B3, DECT, 110 keV	B4, DECT, 110 keV	B5, SECT, 120 kV	B6, DECT, MAR 110 keV	B7, DECT, MAR 70 keV	B8, DECT, MAR 110 keV	B9, DECT, MAR 70 keV	B10, SECT, 120 kV	B11, DECT, 110 keV	B12, DECT, 70 keV	B13, Reference, 120 kV
	Steel		Titanium		Steel		Titanium		PMMA				
Number of delineations	Structure 1	2	2	3	4	4	4	4	4	4	4	4	4
	Structure 2	4	3	2	2	4	3	3	3	3	4	4	4
	Structure 3	0	0	0	3	1	3	3	3	3	4	4	4
	Structure 4	4	4	4	4	4	3	3	3	3	4	4	4
	Structure 5	2	2	2	4	4	4	4	4	4	4	4	4
Dice similarity coefficient [max min]	Structure 1	0.78 0.29	0.84 0.80	0.81 0.43	0.88 0.85	0.90 0.84	0.88 0.86	0.89 0.84	0.89 0.86	0.89 0.87	0.87 0.80	0.90 0.89	0.95 0.90
	Structure 2	0.82 0.74	0.78 0.73	0.31 0.15	0.82 0.82	0.83 0.76	0.77 0.50	0.80 0.52	0.76 0.39	0.76 0.38	0.88 0.85	0.89 0.87	0.92 0.89
	Structure 3				0.79 0.57	0.25 0.48	0.87 0.48	0.83 0.47	0.82 0.37	0.80 0.41	0.91 0.88	0.90 0.84	0.88 0.80
	Structure 4	0.81 0.46	0.80 0.71	0.78 0.42	0.77 0.60	0.82 0.78	0.79 0.64	0.78 0.70	0.82 0.79	0.84 0.80	0.83 0.81	0.87 0.84	0.84 0.76
	Structure 5	0.78 0.74	0.84 0.84	0.82 0.79	0.85 0.76	0.84 0.79	0.88 0.82	0.87 0.84	0.85 0.81	0.88 0.83	0.87 0.82	0.89 0.79	0.89 0.84
Hausdorff distance [mm] [max min]	Structure 1	28.5 15.9	12.2 9.3	24.5 7.9	15.7 5.9	13.9 4.9	9.3 5.4	10.5 5.5	8.3 5.3	7.3 4.6	6.5 3.7	7.3 3.5	3.8 2.9
	Structure 2	13.2 7.3	10.4 9.4	22.4 10.0	10.7 5.0	10.7 7.7	14.7 8.3	10.4 5.9	14.4 8.1	14.0 8.1	5.9 3.5	4.8 3.9	6.7 4.7
	Structure 3				7.8 7.7	24.6	8.3 4.5	9.5 8.2	13.7 6.7	12.2 9.2	5.6 3.9	6.7 3.8	8.8 5.7
	Structure 4	8.0 3.8	9.0 3.5	7.5 3.9	7.5 4.5	4.3 3.1	7.5 4.1	5.0 4.4	5.0 3.0	5.0 3.8	3.7 2.8	4.0 2.9	4.6 3.5
	Structure 5	15.5 11.7	6.8 6.6	8.8 5.7	17.5 7.5	8.3 5.4	14.7 4.2	8.3 5.3	10.3 6.8	7.6 6.1	5.9 3.7	6.4 3.0	5.1 3.3

## Funding sources

This work was supported by grants from the King Gustav V Jubilee Clinic Cancer Research Foundation (2014:46, 2015:40, 2016:095), the Healthcare sub-committee, Region Västra Götaland (Hälso- och sjukvårdsutskottet, VGFOUREG-475621, VGFOUREG-557261) and the Healthcare Committee, Region Västra Götaland (Hälso- och sjukvårdsstyrelsen, VGFOUREG-658911).

## Conflict of interest statement

None of the authors have any conflict of interest.

## Acknowledgements

The authors would like to thank Ninni Drugge for assistance with the acquisition of the CT images on the SECT scanner and Anastasios Papadopoulos MD, and Charlotte Alverbratt (née Månsson) MD for delineating structures.

## Appendices A and B. Supplementary data

Supplementary data to this article can be found online at <https://doi.org/10.1016/j.phro.2019.01.001>.

## References

- [1] Barrett JF, Keat N. Artifacts in CT: recognition and avoidance. *RadioGraphics* 2004;24:1679–91. <https://doi.org/10.1148/rg.246045065>.
- [2] Schmidt MA, Payne GS. Radiotherapy planning using MRI. *Phys Med Biol* 2015;60:R323–61. <https://doi.org/10.1088/0031-9155/60/22/R323>.
- [3] Huang JY, Followill DS, Howell RM, Liu X, Mirkovic D, Stingo FC, et al. Approaches to reducing photon dose calculation errors near metal implants. *Med Phys* 2016;43:5117–30. <https://doi.org/10.1118/1.4960632>.
- [4] Giantsoudi D, De Man B, Verburg J, Trofimov A, Jin Y, Wang G, et al. Metal artifacts in computed tomography for radiation therapy planning: dosimetric effects and impact of metal artifact reduction. *Phys Med Biol* 2017;62:R49–80. <https://doi.org/10.1088/1361-6560/aa5293>.
- [5] Gjestebly L, De Man B, Jin Y, Paganetti H, Verburg J, Giantsoudi D, et al. Metal artifact reduction in CT: where are we after four decades? *IEEE Access* 2016;4:5826–49. <https://doi.org/10.1109/ACCESS.2016.2608621>.
- [6] Lee YH, Park KK, Song H-T, Kim S, Suh J-S. Metal artefact reduction in gemstone spectral imaging dual-energy CT with and without metal artefact reduction software. *Eur Radiol* 2012;22:1331–40. <https://doi.org/10.1007/s00330-011-2370-5>.
- [7] Huang JY, Kerns JR, Nute JL, Liu X, Balter PA, Stingo FC, et al. An evaluation of three commercially available metal artifact reduction methods for CT imaging. *Phys Med Biol* 2015;60:1047–67. <https://doi.org/10.1088/0031-9155/60/3/1047>.
- [8] Pettersson, Erik. Exploring the usage of fast kV-switching dual-energy CT for external photon beam radiotherapy treatment planning (M.Sc. thesis), Department of Radiation Physics, Sahlgrenska Academy at University of Gothenburg, Gothenburg; 2015.
- [9] Dunet V, Bernasconi M, Hajdu SD, Meuli RA, Daniel RT, Zerlauth J-B. Impact of metal artifact reduction software on image quality of gemstone spectral imaging dual-energy cerebral CT angiography after intracranial aneurysm clipping. *Neuroradiology* 2017;59:845–52. <https://doi.org/10.1007/s00234-017-1871-6>.
- [10] Yu L, Leng S, McCollough CH. Dual-Energy CT–Based Monochromatic Imaging. *AJR Am J Roentgenol* 2012;199:9–15. <https://doi.org/10.2214/AJR.12.9121>.
- [11] Li B. Dual-energy CT with Fast-kVp Switching and Its Applications in orthopedics. *OMICS. J Radiology* 2013;02. <https://doi.org/10.4172/2167-7964.1000137>.
- [12] Cha J, Kim H-J, Kim ST, Kim YK, Kim HY, Park GM. Dual-energy CT with virtual monochromatic images and metal artifact reduction software for reducing metallic dental artifacts. *Acta Radiol* 2017;58:1312–9. <https://doi.org/10.1177/0284185117692174>.
- [13] Ohira S, Karino T, Ueda Y, Nitta Y, Kanayama N, Miyazaki M, et al. How well does dual-energy CT with fast kilovoltage switching quantify CT number and iodine and calcium concentrations? *Acad Radiol* 2018;25(4):519–28. <https://doi.org/10.1016/j.acra.2017.11.002>.
- [14] Kovacs DG, Rechner LA, Appelt AL, Berthelsen AK, Costa JC, Friberg J, et al. Metal artefact reduction for accurate tumour delineation in radiotherapy. *Radiother Oncol* 2018;126:479–86. <https://doi.org/10.1016/j.radonc.2017.09.029>.
- [15] Hsieh J, Nett B, Yu Z, Sauer K, Thibault J-B, Bouman CA. Recent advances in CT image reconstruction. *Curr Radiol Rep* 2013;1:39–51. <https://doi.org/10.1007/s40134-012-0003-7>.
- [16] Dice LR. Measures of the amount of ecologic association between species. *Ecology* 1945;26:297–302. <https://doi.org/10.2307/1932409>.
- [17] Hausdorff F. *Grundzüge der Mengenlehre*. Leipzig, Germany: Verlag von Veit & Company; 1914.
- [18] Gossner J. *Computed tomography of the prostate – A review*. *Internet J Radiol* 2012;14:1–7.
- [19] Vinod S, Jameson MG, Min M, Holloway LC. Uncertainties in volume delineation in radiation oncology: A systematic review and recommendations for future studies. *Radiother Oncol* 2016;121:169–79. <https://doi.org/10.1016/j.radonc.2016.09.009>.